Alternative Routes for Entry of HgX_2 into the Active Site of Mercuric Ion Reductase Depend on the Nature of the X Ligands†

Stefan Engst* and Susan M. Miller*

Department of Pharmaceutical Chemistry, University of California, San Francisco, California 94143-0446

Received November 10, 1998

ABSTRACT: Wild-type mercuric ion reductase (CCCC enzyme) possesses four cysteines in each of its Hg(II) binding sites, a redox-active pair and a C-terminal pair. Mutation of the C-terminal cysteines to alanines (CCAA enzyme) leads to a loss of steady-state mercuric ion reductase activity using $Hg(SR)_2$ substrates. However, CCCC and CCAA enzymes exhibit an equally high rate of binding and turnover using $HgBr_2$ as substrate under pre-steady-state conditions [Engst and Miller (1998) *Biochemistry 37*, 11496−11507.]. Since the ligands in these HgX_2 substrates differ both in size and in affinity for Hg(II), one or both of these properties may contribute to their different reactivities with CCAA enzyme. To further explore the importance of these two properties, we have examined the pre-steady-state reactions of CCCC and CCAA with $Hg(CN)_2$, which has small, high-affinity ligands, and with $Hg(Cys)_2$, which has bulky, high-affinity ligands. The results indicate that HgX_2 substrates with small ligands can rapidly access the redox-active cysteines in the absence of the C-terminal cysteines, but those with large ligands require the C-terminal cysteines for rapid access. In addition, it is concluded that the C-terminal cysteines play a critical role in removing the high-affinity ligands before Hg(II) reaches the redox-active cysteines in the inner active site, since direct access of HgX_2 substrates with high-affinity ligands leads to formation of an inhibited complex. Consistent with the results, both a narrow channel leading directly to the redox-active cysteines and a wider channel leading to the redox-active cysteines via initial contact with the C-terminal cysteines can be identified in the structure of the enzyme from *Bacillus sp.* RC607.

The extreme toxicity of mercurials and mercuric ion to living systems is mainly caused by the high affinity of Hg(II) for the thiol(ate) function (log $K_f \sim 40$ for $Hg(Cys)_2$, (*1*)). To prevent the detrimental effects of this heavy metal toxin, many bacterial species have evolved a sophisticated and highly regulated detoxification system in which mercurials and Hg(II) are actively transported into the intracellular space, where ultimate reduction of Hg(II) to the much less toxic Hg(0) leads to elimination of the toxin from the cell (*2*). The crucial two-electron reduction step (eq 1) in this pathway is catalyzed by the flavoprotein mercuric ion reductase (MR[1]), a structural homologue of several of the pyridine nucleotide−disulfide oxidoreductase enzymes.

$$Hg(SR)_2 + NADPH + H^+ \rightarrow Hg^0 + NADP^+ + 2RSH \quad (1)$$

Like glutathione reductase and other members of this family, homodimeric MR has two active sites, each with an FAD cofactor sandwiched between the pyridine nucleotide binding site and a redox-active disulfide (cysteines 135 and 140 in MR from *Pseudomonas aeruginosa* Tn*501*). However, along with its distinctive catalytic activity, MR possesses a uniquely conserved second pair of cysteines (C-terminal pair) that lie near the redox-active cysteines in the active site of the opposite monomer (cysteines 557′ and 558′ in Tn*501*) (*3*−*5*). This C-terminal pair of cysteines does not undergo redox changes at a catalytically relevant rate and is required in its reduced state for full catalytic activity in standard steady-state assays using $Hg(SR)_2$ substrates (*3*). In the presence of the reducing substrate NADPH, the predominant form of the enzyme is an EH_2·NADPH complex with its FAD oxidized and all four cysteines reduced (*6*) (Scheme 1). Consistent with the dominance of this species, reduction of Hg(II) only occurs at a catalytically relevant rate when both substrates are present in an EH_2·NADPH·Hg(II) complex (*7*). Other EH_2 forms (e.g., EH_2·$NADP^+$) can bind Hg(II) and reduce it slowly (ref *8;* Engst and Miller, unpublished observations), but rapid reduction is not observed (*7*). Thus, all four reduced cysteines, together with the two tyrosines shown in Scheme 1 (*4, 9*) (193 and 534′ in Tn*501*), are believed to be involved in the pathway for binding and reduction of the metal ion substrate.

Our current understanding of the roles of the cysteines in this pathway stems largely from studies of a series of single, double, and triple Cys to Ala mutants of the Tn*501* enzyme. Cellular resistance to Hg(II) is only observed with wild-type

† This work was supported by grants from NIGMS (GM50670), The Petroleum Research Foundation of the American Chemical Society (ACS-PRF 27532G4), and the UCSF Academic Senate.

* To whom correspondence should be addressed. (S.M.M.) Phone: 415-476-7155. Fax: 415-476-0688. E-mail: smiller@cgl.ucsf.edu. (S.E.) E-mail: engst@cgl.ucsf.edu.

[1] Abbreviations: CT, charge transfer; EH_2, two-electron-reduced enzyme where the redox-active cysteines are reduced and the flavin oxidized; EH_2·$NADP^+$, two-electron-reduced enzyme complexed with $NADP^+$; EH_2·NADPH, two-electron-reduced enzyme complexed with NADPH; FAD, flavin adenine dinucleotide; ME, 2-mercaptoethanol; MR, mercuric ion reductase; $NADP^+$, nicotinamide adenine dinucleotide phosphate; NADPH, reduced nicotinamide adenine dinucleotide phosphate; RSH, thiol-containing compound such as ME or cysteine; SVD, singular value decomposition.

10.1021/bi982680c CCC: $18.00
Published on Web 02/27/1999

Scheme 1: Organization of Residues in the Hg(II) Binding Site in the EH_2·NADPH Complex of Mercuric Ion Reductase

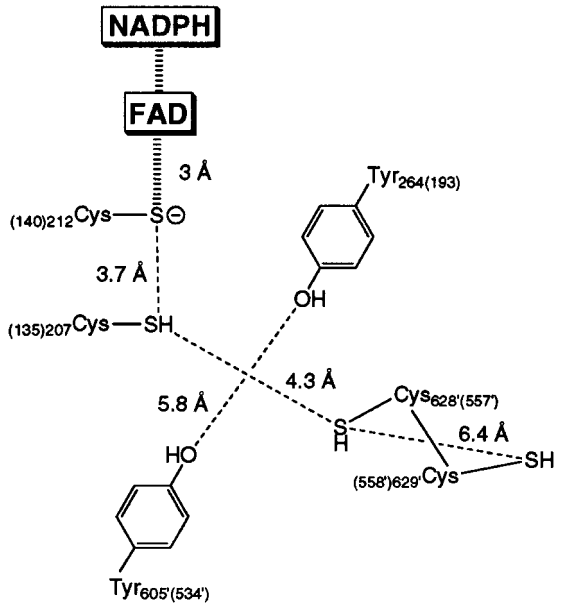

enzyme (*10*−*12*), indicating that all four cysteines are required for sufficient catalytic activity in the cellular milieu. In vitro assays using $Hg(SR)_2$ substrates indicate a requirement for both cysteines of the redox-active pair and at least one of the C-terminal cysteines (C557 preferred) to see significant rates of reduction of Hg(II) [no activity in ACCC,[2] CACC, and CCAA mutants (*10*−*11*); CCCA activity > CCAC (*12*)]. Absence of activity in the CCAA mutant did not appear to be due to lack of access of Hg(II) to the active site since a two-coordinate complex was readily formed in titrations of EH_2 or EH_2·$NADP^+$ with small substrates, such as $HgCl_2$, $HgBr_2$, or $Hg(CN)_2$ (*13*). Thus, it was initially concluded that the two-coordinate Hg(II) complex with C135 and C140 is an inhibited complex and that C557 is required to prevent inhibition by forming either a three-coordinate complex or an alternative two-coordinate complex that undergoes reduction. However, conditions of the binding studies differ from the steady-state assays in both the nature of the HgX_2 substrate and the state of the enzyme since an EH_2·NADPH·Hg(II) complex is the catalytically relevant species during turnover (*7*). Unfortunately, steady-state activity cannot be measured with the alternative HgX_2 substrates because the weaker-liganded complexes ($HgCl_2$ and $HgBr_2$, Table 1) react directly with NADPH to form a covalent Hg(II) adduct (*14*), and the enzyme is inhibited by $Hg(CN)_2$ (*15*). Likewise, titrations of EH_2·NADPH complexes with HgX_2 are not expected to yield useful information if reduction occurs. Thus, a kinetic approach is required to investigate how the catalytically relevant EH_2·NADPH complex of wild-type enzyme differs from the mutants in its reactions with Hg(II) substrates, and whether all HgX_2 substrates react in the same way with these enzymes.

[2] A four-letter code for wild-type and active site mutants which carry one or more mutations in positions 135, 140, 557, and 558 (Tn*501* numbering) of the amino acid sequence is used. For example CCCC denotes wild-type enzyme with cysteines in all four positions; CCAA refers to a double mutant in which cysteines 557 and 558 are both replaced by alanine. (Note, Cys557 and Cys558 in the Tn*501* enzyme were previously referred to as 558 and 559, which is correct if the starting methionine is included. However, 135, 140, 557, and 558 are the consistent set of numbers for the mature protein.)

Table 1: Formation Constants for HgX_n Complexes

X^-	log K_{f1}	log K_{f2}	log K_{f3}	log K_{f4}
Br^- [a]	9.0	8.3	1.4	1.3
CN^- [a]	18.0	16.7	3.8	3.0
Cys^-		40.3[b]	∼1[c]	
GS^-		40.9[b]	3.2[c]	

[a] Taken from ref *17*. [b] Overall formation constants for binding two thiol ligands to Hg(II). Taken from ref *1*. [c] Taken from ref *18*.

To address these questions, we have initiated a series of stopped-flow experiments using diode array detection to characterize the kinetics and spectral intermediates formed during the reaction of EH_2·NADPH complexes of wild-type and several of the Cys to Ala mutants with a variety of HgX_2 complexes. In the first of these studies (*16*), we reported the surprising result that wild-type and CCAA mutant enzymes exhibit equally high rates of binding *and turnover* with $HgBr_2$, indicating no requirement for either C-terminal cysteine in the binding or reduction pathway for this particular HgX_2 substrate. Since bromide differs from the steady-state thiol ligands in both size and affinity for Hg(II) (Table 1), either or both factors may allow $HgBr_2$ to circumvent the normal pathway for binding and reduction of $Hg(SR)_2$ substrates that appears to require the C-terminal cysteines. To shed further light on how the properties of the ligand X affect binding and reduction of HgX_2, we present studies of the reaction of EH_2·NADPH complexes of wild-type and mutant enzymes with $Hg(Cys)_2$ and $Hg(CN)_2$ substrates in which all of the ligands are high-affinity (Table 1) but differ substantially in size. Results of these studies are combined with an analysis of the protein structure to develop a molecular picture suggesting alternative pathways for binding of HgX_2 substrates that lead to reduction and/or inhibition depending on the nature of the ligand X.

MATERIALS AND METHODS

L-Cysteine of the highest grade available was obtained from Sigma. $Hg(Cys)_2$ was made by addition of a solution of L-Cys to a solution of $HgBr_2$ to a final Cys/Hg(II) ratio of 2:1. Color graphics were generated on a Silicon Graphics computer using the program Insight II, followed by further manipulation using Photoshop 5.0 and Quark 4.0. All other procedures were described in detail in previous work (*16*).

RESULTS AND DICUSSION

Postulated Binding Modes from Structural Data. Predictions of potential protein complexes and a mechanism for binding of Hg(II) rely on knowledge of its coordination chemistry in solution. As summarized in Table 1, Hg(II) exhibits significantly higher affinities for association with its first two ligands indicating a preference for linear two-coordination. The magnitudes of the formation constants (even for the weaker bromide ligand) indicate that exchange of ligands in an HgX_2 complex would be quite slow if ligand dissociation occurred first, while weakly bound third and fourth ligands could dissociate rapidly. Consistent with this, $Hg(SR)_2$ complexes have been shown to undergo rapid ligand exchange [$\geq 1000\ s^{-1}$, (*18*)] through transient formation of

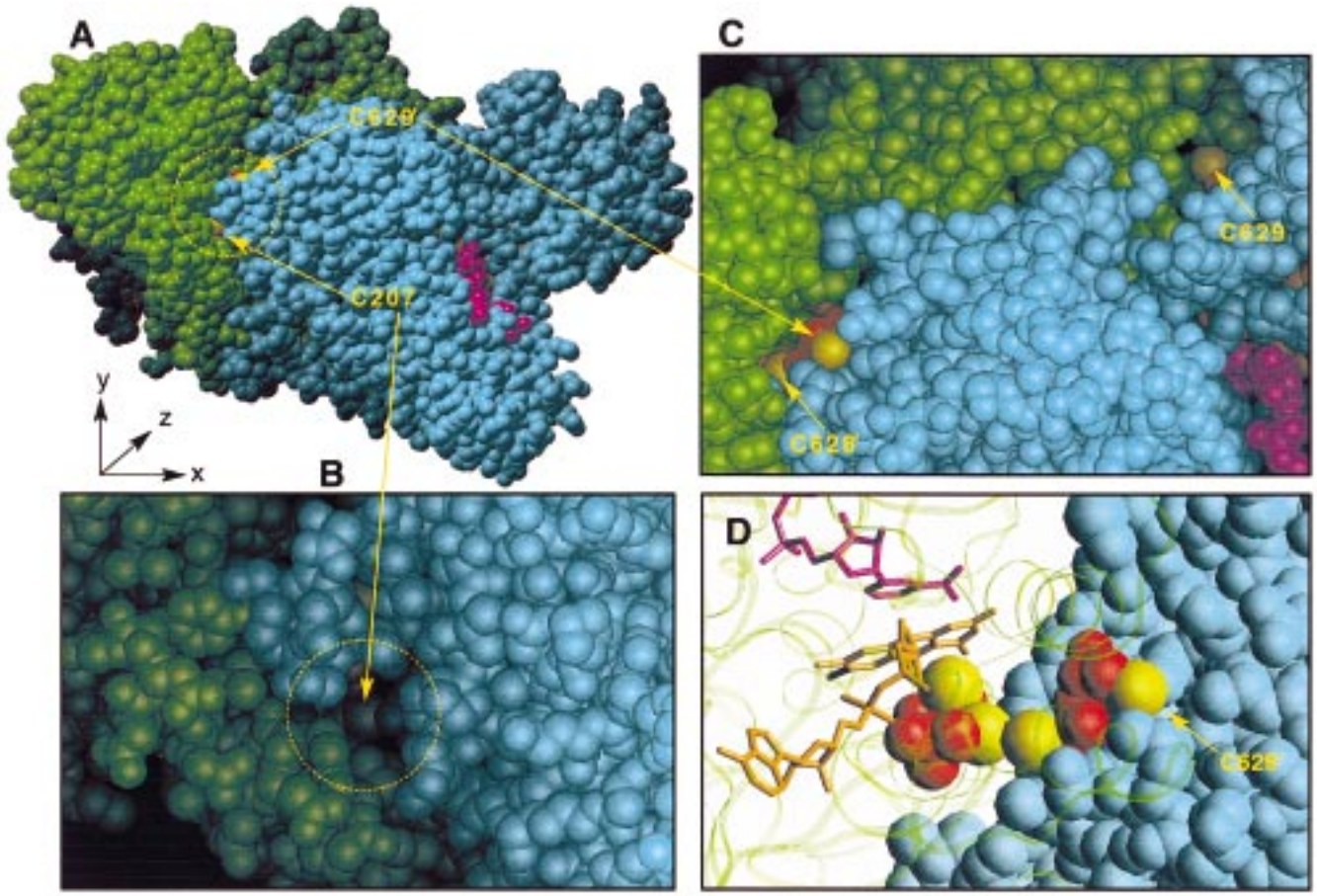

FIGURE 1: Spatial arrangement of active site cysteines in mercuric ion reductase (from *Bacillus sp*. RC607). Color coding: The two subunits are in green and blue. Pyridine nucleotide and flavin are pink and orange, respectively. All atoms of the active site cysteines are red except the sulfurs, which are yellow. (Panel A) Overview of the MR dimer. The circled area denotes the binding region for the metal substrate at the interface of the two subunits with C207 and C629′ (C135 and C558′ in Tn*501*) as the most surface-exposed cysteine residues. (Panel B) Rotation of the molecule by about 30°, counterclockwise around both the *y*-axis and the *x*-axis yields a view into a deep (≥10 Å), narrow channel at the bottom of which lies C207. (Panel C) Clockwise rotation of panel A around the *x*-axis by about 30° gives a view of the much wider C-terminal channel with C629′ as the most exposed cysteine residue. More than 6 Å deeper inside the channel, the sulfur atom of C628′ (C557′ in Tn*501*) can be seen. In the upper right-hand corner, C629 of the second active site is shown. (Panel D) This view shows the active site as seen through the green subunit (depicted as a ribbon). The sulfurs, from right to left [i.e., with decreasing distance from the isoalloxazine ring of the flavin (orange)], belong to C629′, C628′, C207, and C212 (C140 in Tn*501*). This view clearly shows that access to the sulfur of C629′ is not obstructed by residues belonging to the green subunit. In this image the channel depicted in panel B lies below the sulfur of C207 and opens in the $+z$ direction.

$[Hg(SR)_3]^-$ complexes that can persist with a trigonal planar geometry at higher thiol concentrations (*19*). Thus, the pathway for binding of HgX_2 substrates to the active site cysteines in MR is expected to involve formation of a series of two-coordinate complexes via transient three-coordinate ligand exchange complexes to displace the two X ligands and ultimately transfer Hg(II) to either a two- or three-coordinate final complex (depending on the active site topology) that undergoes reduction.

Examination of the structure of the NADPH-reduced enzyme from *Bacillus sp*. RC607 [Figure 1 and Scheme 1; (*4*)] suggests two potential pathways for access of HgX_2 substrates to the active site of wild-type enzyme, a C-terminal route and a bypass route. In the C-terminal pathway, HgX_2 would enter via a wide channel (Figure 1C) and undergo ligand exchange reactions first with C629′ (C558′) followed by C628′ (C557′) to displace both X ligands and form the first, or *outer*, of three successive two-coordinate thiol complexes with the protein (Scheme 2). Although the orientation and S−S distance between these groups in the reduced enzyme appear unsuitable for formation of a two-coordinate complex [optimal S−S distance: 4.7−4.8 Å (*20*−*21*) versus 6.4 Å in the MR structure (*4*), Scheme 1], the structure of the oxidized enzyme reveals a disulfide between the two indicating a degree of flexibility in the C-terminal region sufficient to allow formation of the complex with Hg(II) (*4*). Reorientation of this *outer* complex to allow attack of C207 (C135) would transfer Hg(II) to a *middle* complex with nearly optimal two-coordinate liganding by C207 (C135) and C628′ (C557′) and possible weaker liganding by two tyrosine hydroxyls, giving an overall distorted tetrahedral geometry. The competitive inhibitor Cd(II) was found in this binding site in another structure of the protein (*4*). Further dynamic motion should allow a final transfer from the *middle* to an *inner* two-coordinate complex involving C212 (C140) and C207 (C135) that lies adjacent to the electron-mediating FAD.

In the bypass route, HgX_2 would enter via a much narrower channel (Figure 1B) leading to an initial encounter with C207 (C135) and displacement of the first X ligand.

Scheme 2: Proposed C-terminal Path for Binding of HgX_2 and Transfer into the Inner Active Site

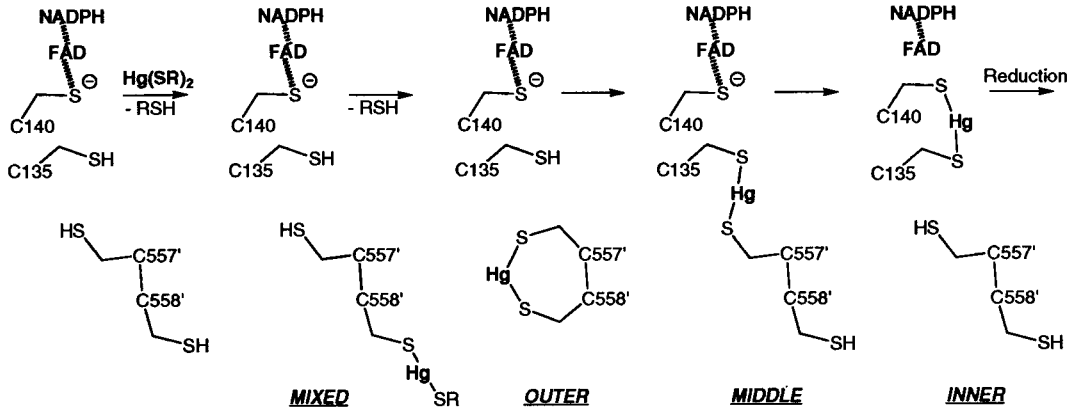

Depending on the dynamic motion of the active site residues, particularly the C-terminal region, exchange of the second X ligand could involve reaction with C628′ (C557′) to give the *middle* complex followed by transfer to the *inner* complex, or it could involve reaction with C212 (C140) to give the *inner* complex directly. Although the static picture suggests that reaction with C628′ (C557′) may be sterically favored, reaction with C212 (C140) may predominate because its deprotonated sulfur ($pK_a = 5$) should be a better nucleophile (*18*). In the CCAA mutant enzyme, the latter version of the bypass route involving C135 and C140 is the only pathway available for binding of HgX_2 substrates. Thus, comparison of the reactions of wild-type and CCAA enzymes with different HgX_2 ligands should provide insight into the viability of these pathways, and hence, the roles of the C-terminal cysteines, as the properties of X vary.

Expected Spectral Perturbations. In the data that follow, the reactions of the EH_2·NADPH complexes with HgX_2 substrates are monitored by changes in the UV−vis spectrum. As indicated in Scheme 1, the thiolate anion of C140 lies in close proximity to the oxidized isoalloxazine ring of the FAD cofactor and interacts with it in a charge-transfer (CT) donor/acceptor pair. (This interaction prevents reduction of FAD by bound NADPH.) From the other side of the ring, NADPH also acts as a charge-transfer donor with FAD as the acceptor. Both interactions contribute nearly equally to the long wavelength absorbance at about 520 nm in the spectrum of EH_2·NADPH (see Figure 2); thus, loss of absorbance at 520 nm can be indicative of either consumption of NADPH or neutralization of the negative charge on the C140 sulfur. However, the two processes can be distinguished by two other features. Consumption of NADPH also leads to a loss of absorbance at 340 nm and a shift in the λ_{max} of the remaining thiolate/FAD CT band but no change in the resolution of the flavin main band (450 nm region). In constrast, neutralization of the charge on the C140 sulfur due to binding of Hg(II) results in dramatic resolution of the flavin main band (450 nm region) concomitant with a similar shift in the λ_{max} of the remaining NADPH/FAD CT band, but gives no loss of absorbance at 340 nm. When the charge is neutralized *and* NADPH is consumed, no CT interactions and, therefore, no long wavelength bands remain. With these properties of EH_2·NADPH, the main aspects of the reaction we expect to monitor are (1) the arrival of Hg(II) at the C140 sulfur in either a transient three-coordinate or two-coordinate *inner* complex, and (2) the timing of electron transfer from NADPH if it occurs. Binding of Hg(II) in the *middle* complex or to C135 alone may perturb the CT interaction because of the proximity of C135 to C140 (see below); however, binding in the *outer* complex is not expected to be directly observable in these studies.

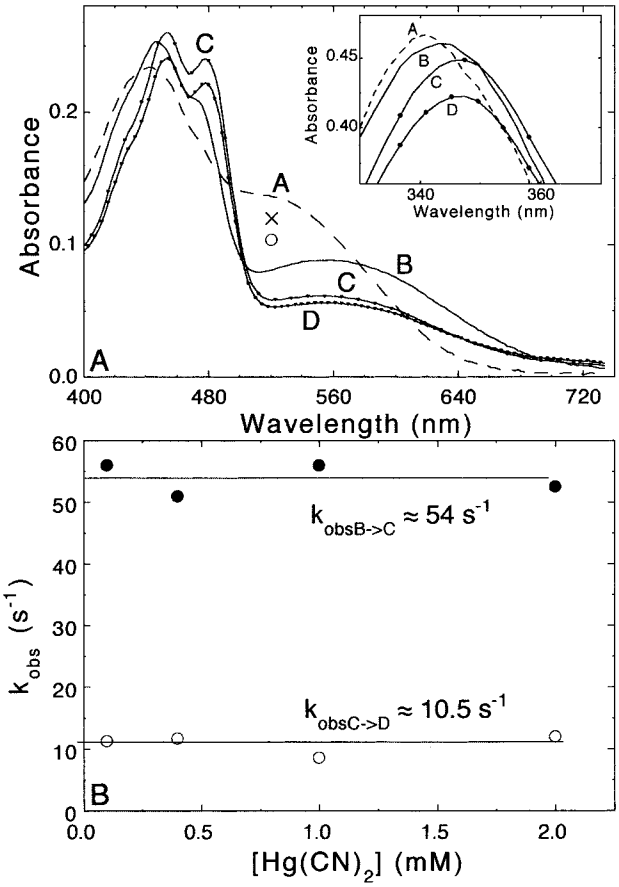

FIGURE 2: (Panel A) Results of rapid mixing of the EH_2·NADPH (29.6 μM stoichiometric complex) form of the CCAA mutant (curve A) with 1 mM $Hg(CN)_2$ (final concentrations) in a stopped-flow spectrophotometer. Curves B (deadtime spectrum), C, and D are the spectral species obtained from singular value decomposition (SVD) of the raw data and a fit to two consecutive exponentials using the program ProK from Applied Photophysics. Apparent rate constants of 56 and 9.2 s^{-1} were obtained from analysis of a time interval of 1 s. Deadtime changes at 521 nm obtained in separate reactions using 30 and 100 μM $Hg(CN)_2$ (final concentrations) are indicated by the cross and open circle, respectively. The *inset* depicts the 340 nm region. (Panel B) shows the concentration dependence of the rate constants for the second and third phases.

Table 2: Estimated Rate Constants[a] for Binding of Hg(II) Compounds to Wild-Type and C → A Active Site Mutant Mercuric Ion Reductases

HgX_2	ACAA	CCAA	CCCA	CCCC
$HgBr_2$	$\sim 6.3 \times 10^4$ [b]	$\sim 8 \times 10^6$ [d]		$\sim 8 \times 10^6$ [e]
$Hg(CN)_2$	$\sim 5 \times 10^2$ [c]	$\geq 3 \times 10^6$ [c]		$\geq 3 \times 10^6$ [e]
$Hg(Cys)_2$		$\sim 2.7 \times 10^2$ [c]	$\sim 3.7 \times 10^2$ [c]	$\geq 4.4 \times 10^5$ [c]

[a] Units for all constants are M^{-1} s^{-1}. [b] Values were obtained from the slope of a linear plot of k_{obs} versus $[HgBr_2]$ using data from ref *16*. [c] This work. [d] From ref *16*. [e] An identical value to that in the CCAA mutant was estimated, on the basis of the same extent of binding-related spectral changes occurring during the deadtime of the stopped-flow measurement for both enzymes.

Effect of the Affinity of X for Hg(II) on Kinetics of Binding and Reduction of HgX_2

As summarized above, the rapid reaction of the CCAA enzyme with $HgBr_2$ versus the absence of reaction with $Hg(SR)_2$ substrates must be due to differences in the size and/or affinity of the associated ligands. To dissect the importance of these two factors, we have examined the reactivities of two substrates that provide stepwise changes in the two properties as compared to $HgBr_2$. For the first step, $Hg(CN)_2$ was chosen to maintain the size of the ligands (C−N bond length in CN^- is ~1.15 Å versus ionic radius of 1.14 Å for Br^-; ref *22*) while dramatically increasing the ligand affinity to a value near that of thiols (Table 1).

Reaction of $Hg(CN)_2$ with CCAA and ACAA Enzymes. In our previous study (*16*), comparison of the second-order rate constants associated with the quenching of the thiolate/FAD CT absorbance for CCAA versus ACAA enzymes (Table 2) indicated that $HgBr_2$ reacts with CCAA EH_2·NADPH in an initial rate-limiting step with the C135 sulfur followed by rapid reaction (kinetically undetectable) with the C140 sulfur to yield a fully quenched and resolved Hg(II) complex with λ_{max} of 452 nm for the flavin main band. This initial complex undergoes a rapid red shift in both the flavin main band ($\lambda_{max} = 458$ nm) and the remaining NADPH/FAD CT band to give a final *inner* complex that undergoes reduction. Since ligand exchange reactions at Hg(II) proceed through transient three-coordinate species, it was proposed that the initial complex with λ_{max} of 452 nm could be a three-coordinate species, and the red shift results from conformational and/or electronic changes in the *inner* complex associated with dissociation of the remaining bromide ligand (*16*).

The spectral changes in the reaction of CCAA EH_2·NADPH with $Hg(CN)_2$ suggest that the order of reaction with C135 and C140 is the same, but the kinetic course and final outcome are somewhat different. Analysis of data obtained over a time interval of 1 s yields the best fit for a model with three exponentials and spectra for the apparent intermediates shown in Figure 2A. At high $Hg(CN)_2$ concentrations (≥0.5 mM), the first phase of the reaction is complete within the deadtime of the measurement and results in curve B. At lower $Hg(CN)_2$ concentrations, the extent of reaction occurring during the deadtime is less (ca. 25% completion at 30 μM and 60% completion at 100 μM $Hg(CN)_2$), indicating involvement of a second-order binding step in this phase of the reaction. Although the concentration dependence was not determined explicitly, the magnitude of the second-order rate constant for initial binding of $Hg(CN)_2$ to the enzyme must be large enough to account for the observed extent of reaction. Thus, a *minimal* value of 3×10^6 M^{-1} s^{-1} is estimated for $k_{binding}$ from the 60% completion observed at 100 μM $Hg(CN)_2$ and the average deadtime of the measurement of 2.5 ms. This value is comparable to that observed for the reaction of $HgBr_2$ with the enzyme (Table 2), suggesting a similar accessibility of this small HgX_2 substrate to the redox-active cysteines.

In contrast to the similar rate of access, the spectrum of this first intermediate (curve B) and the behavior in the subsequent reactions differ substantially from those in the $HgBr_2$ reaction. Instead of becoming fully quenched and resolved during the second-order binding step, the thiolate/FAD CT band and main band resolution only reach about 50% completion in the first phase. A red shift in the λ_{max} of the remaining thiolate/FAD CT band is consistent with formation of a mixed $Hg(S_{135})(CN)$ complex in the unquenched sites, since similar shifts have previously been observed in EH_2 forms of the enzyme when C135 reacts with other reagents, such as in the reaction of EH_2 with iodoacetamide (*23*) and in the initial phase of the reaction of CCAA EH_2·$NADP^+$ with $Hg(CN)_2$ (unpublished observations). The remainder of the thiolate/FAD CT quenching and main band resolution occurs in a second, $[Hg(CN)_2]$-independent phase (Figure 2A, B → C) with an average value for $k_{obs,B\rightarrow C}$ of 54 s^{-1} (Figure 2B). Thus, the reaction of the C140 thiolate with the initial mixed $Hg(S_{135})(CN)$ complex appears to occur biphasically, with half reacting in the deadtime (≥700 s^{-1}) and the other half at 54 s^{-1}. In principle, the rapid reaction of C140 leading to the ~50% quenching could be explained by an equal reactivity of the C135 and C140 sulfurs with the entering HgX_2 substrate. Evidence against this idea includes the structural data (Figure 1), which indicate that C135 should be the initial point of contact via either entry route, and a measured rate constant for direct reaction of $Hg(CN)_2$ with C140 in the ACAA enzyme that is 4 orders of magnitude lower than that for the reaction with CCAA (data not shown) (Table 2). A second explanation to consider is the possibility of an asymmetric dimer. A number of examples of different reactivities of the two active sites in homodimeric MR have previously been reported (*24*). This may be another instance in which the orientation of the initial mixed $Hg(S_{135})(CN)$ complex is substantially different in the two sites allowing rapid reaction of C140 in one site but not in the other (see below). However, a somewhat simpler and more appealing scenario based on the differing properties between bromide and cyanide anions is shown in Scheme 3. In this case, it is proposed that the C140 sulfur is fully accessible to the initial mixed complex in both sites and can rapidly react with it to form a three-coordinate intermediate, just as was proposed in the reaction with $HgBr_2$. However, the remaining cyanide ligand in this case has a much higher affinity for Hg(II) (as compared to the remaining bromide in the previous case), and perhaps more importantly, is quite basic compared to bromide ($pK_{aHBr} = -8.7$; $pK_{aHCN} = 9.2$). Since bromide is a very stable anion and has a much lower affinity than the two thiols in the three-coordinate complex, its dissociation should be the favored path for decomposition of the intermediate. On the other hand, the affinity of the cyanide ligand is not that much lower than that of the two thiols (Table 2), and the basicity of the leaving cyanide anion ($pK_{aHCN} = 9.2$) is much higher than that of the C140 thiolate anion ($pK_a \leq 5$; ref *25*). If a proton is not *optimally* located

Scheme 3: Proposed Mechanism for Binding of $Hg(CN)_2$ to CCAA EH_2·NADPH

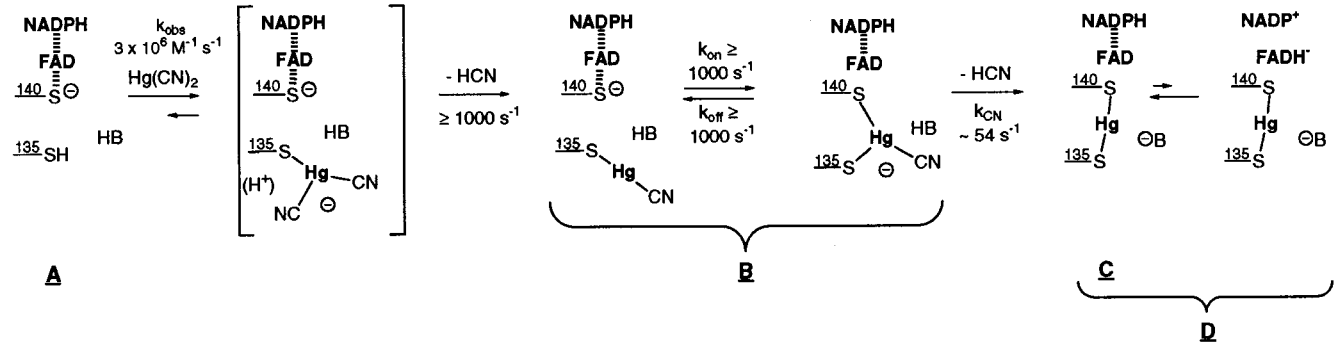

to assist dissociation of cyanide, dissociation of the C140 sulfur would likely be the favored path for decomposition of the three-coordinate intermediate (k_{off} in Scheme 3), which would lead to a return of thiolate/FAD CT absorbance. Similar rate constants for association and dissociation of the C140 sulfur to and from the two-coordinate mixed $Hg(S_{135})$-(CN) and three-coordinate complexes, respectively (i.e., $K_{eq} \approx 1$ in Scheme 3) would account for the approximate 50% quenching observed in intermediate B; the rapid establishment of the equilibrium in the deadtime would indicate magnitudes for these rate constants of $\geq 1000\ s^{-1}$, consistent with the measured rate of dissociation of glutathione anion from a $[Hg(GS)_3]^-$ species in solution (*18*) and the undetectably rapid association of C140 with the mixed $Hg(S_{135})$-(Br) complex in our previous study (*16*). In this scenario then, "species B" is the equilibrium mixture of two- and three-coordinate species and conversion of "B" to an *inner* complex C, as monitored by the further loss of thiolate/FAD CT absorbance, is limited by the rate constant for dissociation of cyanide from the three-coordinate complex. Thus, $k_{obsB\rightarrow C} = k_{on}k_{CN}/(k_{off} + k_{CN})$, and $k_{CN} \approx k_{obsB\rightarrow C} = 54\ s^{-1}$ since $k_{on} \approx k_{off} \geq 1000\ s^{-1}$. (Although loss of cyanide should be reversible, the equilibrium appears to lie far to the right, suggesting that the rate for reassociation is much smaller than dissociation and can be neglected.) This value for $k_{obsB\rightarrow C}$ is at least 6-fold lower than the rate constant for the red shift observed in the $HgBr_2$ reaction that was attributed at least in part to dissociation of bromide from that three-coordinate complex.

After formation of the *inner* complex C, a third phase occurs (C→D, $k_{obs} \approx 10.5\ s^{-1}$) involving only small decreases in intensity throughout the spectrum (Figure 2A) that are indicative of formation of a small amount (~5−10%) of EH_4·$NADP^+$·Hg(II) from EH_2·NADPH·Hg(II), and suggest a slight increase in the flavin reduction potential to a more positive value upon removal of the negative charge on the C140 sulfur. However, no further consumption of NADPH is observed, indicating that the *inner* complex generated by displacement of this apparently slower dissociating ligand is inhibited toward reduction of the bound Hg(II). Comparison of the spectra of this inner complex formed from $Hg(CN)_2$ with the rapidly reduced *inner* complex formed in the $HgBr_2$ reaction shows that the species are indeed not identical (Figure 3). Although both exhibit spectral properties consistent with the formation of *inner* complexes, the λ_{max} values for both the flavin main band and the CT band are blue-shifted (to higher energy) in the complex derived from $Hg(CN)_2$, indicating a significant difference in the electronic environment of the flavins in these two complexes. In

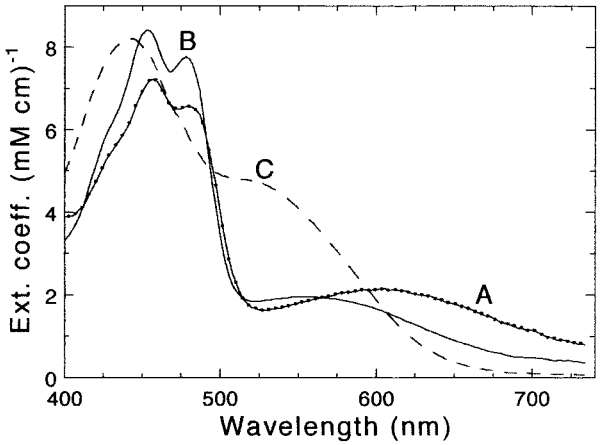

FIGURE 3: Comparison of the spectral properties of the CCAA EH_2·NADPH·Hg(II) complexes obtained after rapid mixing of EH_2·NADPH with $HgBr_2$ (curve A) and $Hg(CN)_2$ (curve B). Curve B is equivalent to curve D in Figure 2. Curve A is taken from a previously published experiment (*16*) where 12.4 μM EH_2·NADPH was mixed with 100 μM $HgBr_2$ (concentrations after mixing). Spectra were normalized by comparison of their respective EH_2·NADPH spectra. Curve C shows the corresponding spectrum of CCAA EH_2·NADPH.

particular, the NADPH/FAD CT band is shifted 55 nm from 605 to 550 nm, not far from its apparent value in the starting EH_2·NADPH complex where there is a full negative charge on the C140 sulfur. This suggests that, although the charge on C140 is quenched (as evidenced by the resolution of the flavin main band), there may still be a negative charge within the Hg(II) binding site, near enough to the flavin to affect its electronic environment. This idea is also consistent with the substantial red shift in the NADPH/FAD CT band (580−605 nm) observed as the three-coordinate complex derived from $HgBr_2$, which should carry a diffuse negative charge $[Hg(S_{135})(S_{140})Br]^-$, is converted to the neutral two-coordinate *inner* complex. Incomplete dissociation of cyanide from the active site could account for this remaining negative charge, but this seems unlikely since it is similar in size to bromide, which clearly is not retained. A more likely alternative source of negative charge is the generation of an anionic active site residue (perhaps one of the tyrosines) resulting from donation of its proton to the basic cyanide anion as it dissociates (Scheme 3). Such a charge would not be generated upon dissociation of the low basicity bromide anion. Further comment on this issue is given below.

Reaction of $Hg(CN)_2$ with CCCC. The spectral changes occurring during the reaction of CCCC EH_2·NADPH with $Hg(CN)_2$ are more complex than those observed for the

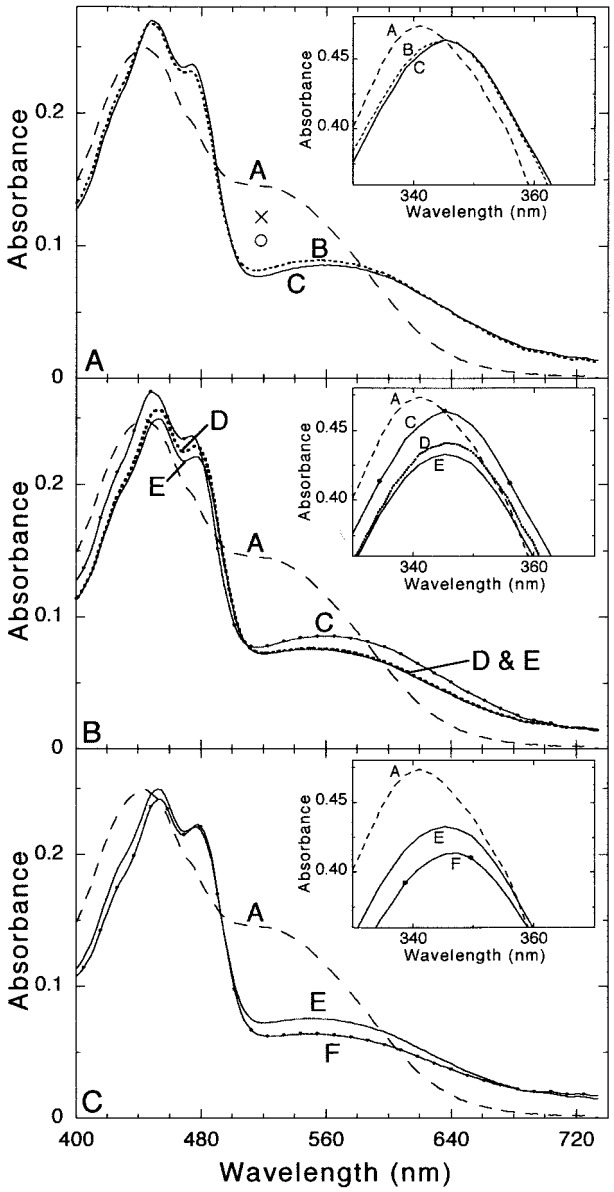

FIGURE 4: Results obtained upon rapid mixing of 29.7 μM CCCC EH_2·NADPH (curve A in each panel) with 1 mM $Hg(CN)_2$ (final concentrations). The *inset* in each panel shows changes in the 340 nm region. (Panel A) Spectrum B was obtained at the stop of flow (deadtime spectrum denoted as 1.28 ms) and spectrum C was obtained at 6.4 ms. (Panel B) Spectrum C is the same as in panel A and, spectra D and E were obtained at 198.4 ms and 1.021 s, respectively. (Panel C) Spectrum E is the same as in panel B and spectrum F was obtained at 19.64 s.

CCAA enzyme and strongly suggest that the substrate reacts via both the C-terminal and bypass pathways described above. In their reactions with 1 mM $Hg(CN)_2$, the enzymes form essentially identical final complexes that are inhibited toward reduction of bound Hg(II) (compare curve D in Figure 2A with curve F in Figure 4C). However, at least two additional phases are apparent during the course of the CCCC reaction. Rather than assuming a specific model for the reaction (e.g., linear versus parallel paths for intermediate formation), raw spectra from selected time points in the reaction are presented in Figure 4 to illustrate the nature of the changes to be considered. Panel A illustrates the presence of the first additional phase in the CCCC reaction. On one hand, the observation of a similar concentration dependence of the changes occurring in the deadtime for the two enzymes (curves B and symbols × & ○ in Figures 2A and 4A) suggests that the binding pathway described in Scheme 3 is equally available in the CCCC enzyme and is limited by a similar second-order rate constant for binding to the C135 sulfur (Table 2). However, the rapid phase quenching of the thiolate/FAD CT band in the CCCC reaction is not quite complete in the deadtime. Rather, a second rapid phase is detectable by the appearance of different sets of isosbestics between the deadtime spectrum (curve B) and the starting enzyme (curve A) versus the deadtime and a spectrum taken 5.12 ms after the stop of flow (curve C in Figure 4A). Although this phase is not sufficiently resolved from the first to determine whether it exhibits a concentration dependence, the rapidity of the reaction and the fact that it leads to further quenching suggest that it reflects an effect of binding of $Hg(CN)_2$ via the C-terminal route (Scheme 2), that is, a route not available in the CCAA enzyme. In principle, the additional quenching could result from direct transfer of Hg(II) to the *inner* complex via the C-terminal route, but only if both the second-order reaction of $Hg(CN)_2$ with the C558′ sulfur and the subsequent two ligand exchange reactions to give the *middle* complex (see Scheme 2) occur more rapidly than the direct second-order reaction of $Hg(CN)_2$ with the C135 sulfur. Alternatively, the additional phase may reflect a perturbation of the initial equilibrium between the mixed $Hg(S_{135})(CN)$ and inner three-coordinate complexes (Scheme 3) toward the three-coordinate species as the *outer* Hg(II) complex is formed via the C-terminal route (Scheme 4). The fact that the final species formed in the reaction is essentially identical to that formed in the CCAA reaction suggests that Hg(II) reaches the C140 sulfur predominantly through the bypass route. This is also supported by the observation of a further phase of quenching of thiolate/FAD CT (C → D in Figure 4B) in a time frame consistent with conversion of intermediate B to C in the CCAA reaction (Figure 2A) that was proposed to result from slow dissociation of a cyanide ligand from the inner three-coordinate complex formed by reaction of $Hg(CN)_2$ via the bypass route (Scheme 3). However, there is a second extra phase in the CCCC reaction (D → E in Figure 4B), not present in the CCAA reaction, that involves a slight loss of resolution in the flavin main band concomitant with no change in the CT band, which is characteristic of conversion of an NADPH/FAD CT band (with the C140 sulfur uncharged) to a thiolate/FAD CT band in the presence of $NADP^+$, such as occurs in the reduction of the disulfide in the E_{ox}·NADPH complex to yield EH_2·$NADP^+$ (*6*). In the current reaction, such a conversion should occur upon transfer of electrons from bound NADPH to Hg(II) bound in an *inner* complex. Thus, the presence of this phase suggests that a small amount of the *inner*-complexed Hg(II) (ca. 5%) does get reduced at a reasonable rate (apparent rate of $3-4\ s^{-1}$) and therefore must be formed via the alternative C-terminal route since no significant reduction was observed in the CCAA reaction. A working model of these competing pathways is summarized in Scheme 4.

Further evidence that $Hg(CN)_2$ reacts at similar rates via both routes in the CCCC enzyme comes from examination of the reaction of the enzyme with only one equivalent of $Hg(CN)_2$. In contrast to the CCAA enzyme, which gives the same inhibited species with both high $Hg(CN)_2$ concentrations and only one equivalent (data not shown), reaction of

Scheme 4: Proposed Competing Paths for Binding of $Hg(CN)_2$ to CCCC EH_2·NADPH

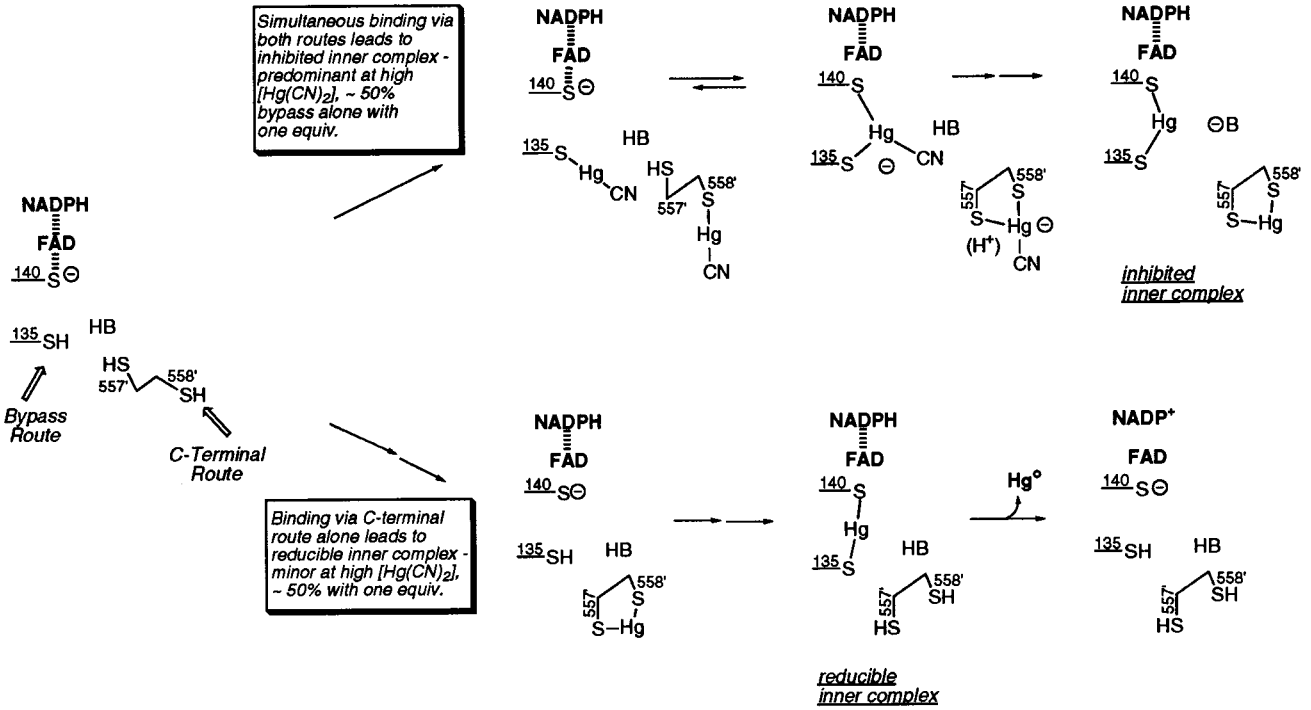

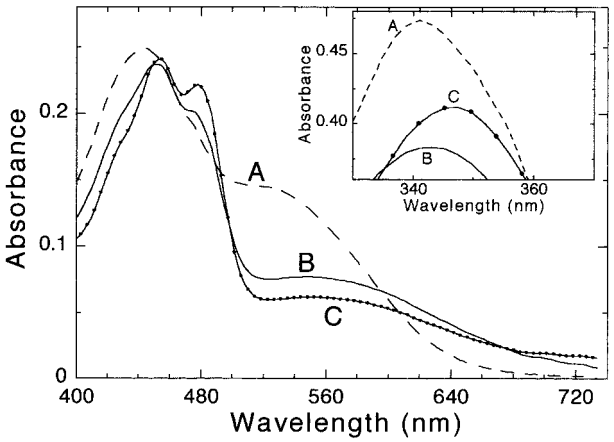

FIGURE 5: Comparison of the final species obtained in the reaction of 29.7 μM CCCC EH_2·NADPH (curve A) with 30 μM (curve B) versus 1 mM (curve C, same as F in Figure 4C) $Hg(CN)_2$ (final concentrations).

CCCC with only one equivalent gives spectral changes consistent with about 50% reduction of the Hg(II). This can be seen by comparison of several features in the final spectra for the 1 mM versus one equivalent reactions shown in Figure 5. First, there is a greater overall decrease in the 340 nm region in the one equivalent reaction with almost none of the substantial shift in λ_{max} observed during formation of the inhibited complex (compare insets, Figure 2A, 4C, and 5). The magnitude of the decrease is consistent with consumption of up to 0.5 equiv of NADPH, indicating that there should be about 50% EH_2·$NADP^+$ remaining that retains thiolate/FAD CT absorbance ($\lambda_{max} = 540-580$ nm, depending on the extent of $NADP^+$ dissociation), and about 50% of an EH_2·NADPH·Hg(II) complex. Partial resolution of the flavin main band is consistent with this and indicates that Hg(II) is bound in an *inner* complex that should have a λ_{max} of about 550 nm if it is the inhibited complex. Both the position and intensity of the remaining CT band are completely consistent with each site retaining only one CT interaction as described. The observation of roughly 50% reduction in the CCCC enzyme, but not in the CCAA enzyme under these conditions, supports the proposal that small HgX_2 substrates can react equally rapidly with the C135 and C558 sulfurs in the two separate pathways. More importantly, however, it also strongly suggests that access via the C-terminal route, which allows exchange (i.e., displacement) of the high-affinity, basic cyanide ligands before Hg(II) reaches the inner active site, is critical for formation of a reducible *inner* Hg(II) complex from a HgX_2 substrate where X is a high-affinity ligand. Another example of this will be found below.

Effect of the Size of X on Kinetics and Reduction of HgX_2

Reaction of $Hg(Cys)_2$ with CCAA. When the ligand X is changed from the small, high-affinity cyanide to a larger, high-affinity thiol ligand, cysteine, some aspects of the reactions are similar, but there are also striking differences. In contrast to the triphasic reaction of CCAA EH_2·NADPH with $Hg(CN)_2$, data for the reaction with high concentrations of $Hg(Cys)_2$ are best fit by a two-step model. Comparison of the spectra of the final species from each reaction suggests that a similar inhibited two-coordinate *inner* complex is formed from both substrates (curve C in Figure 6A and curve D in Figure 2A); however, the kinetics are dramatically different. In contrast to the $Hg(CN)_2$ reaction where quenching of the thiolate/FAD CT is biphasic with the second-order binding phase complete in the deadtime of the reaction (curve B, Figure 2A), very little change occurs in the deadtime of the $Hg(Cys)_2$ reaction. Instead, essentially complete resolution of the flavin main band and quenching of the thiolate/FAD CT band (curve B, Figure 6A) occur in a single phase, limited by the second-order reaction with $Hg(Cys)_2$ (Figure 6B) with a rate constant ($k_{binding} \approx 273$ M^{-1} s^{-1}) that is at least 4 orders of magnitude lower than the initial binding reaction observed with $HgBr_2$ and $Hg(CN)_2$ (Table 2). Clearly

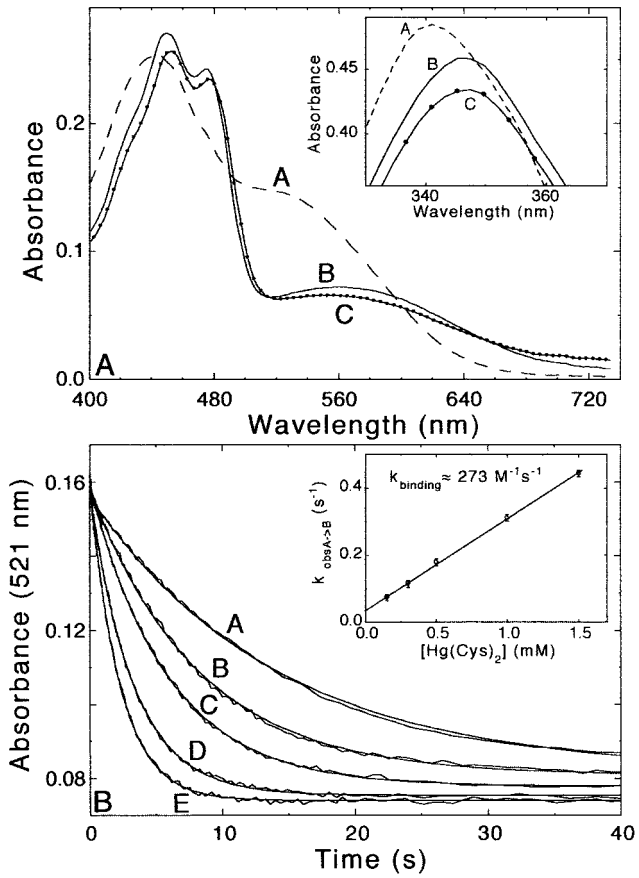

FIGURE 6: (Panel A) Results of rapid mixing of CCAA EH_2·NADPH (29.6 μM stoichiometric complex, curve A) with 1.5 mM $Hg(Cys)_2$ (final concentrations) in a stopped-flow spectrophotometer. *No changes occurred during the deadtime of the measurement*. Curves B and C are the spectral species obtained from SVD of the raw data and a fit to two consecutive exponentials, with apparent rate constants of 0.46 and 0.34 s^{-1}. The *inset* depicts changes in the 340 nm region. Panel B shows kinetic traces at 521 nm with final concentrations of 0.15, 0.3, 0.5, 1, and 1.5 mM $Hg(Cys)_2$ for traces A through E, respectively. The smooth lines represent the best fits to a single exponential. The *inset* shows a plot of the apparent rate constant versus $Hg(Cys)_2$ concentration.

the size of the ligand dramatically decreases accessibility of the $Hg(Cys)_2$ substrate to C135 in the inner active site of this mutated enzyme, consistent with the small size of the bypass channel (Figure 1) that is proposed as the rapid path of entry for the smaller $HgBr_2$ and $Hg(CN)_2$ substrates. Further examination of the structure in Figure 1 argues that, to form an *inner* complex at all from this substrate, the C-terminal region of the protein must undergo substantial "breathing" to allow entry of the larger $Hg(Cys)_2$ via either channel. The fact that the reaction exhibits a second-order concentration dependence indicates that the dynamics of this breathing is not rate-limiting, but suggests that, out of the ensemble of enzyme conformations, the statistical population of enzyme with a sufficiently open conformation is fairly low.

Although the general nature of intermediates in the reaction of CCAA with $Hg(Cys)_2$ is most likely the same as that depicted in Scheme 3 for $Hg(CN)_2$, the requirement for significant reorganization of the C-terminal region could easily alter the position of equilibria and kinetics of the reactions after the initial binding reaction. Thus, the essentially complete quenching of the thiolate/FAD CT band in the slow phase indicates that at least the transient *inner* three-coordinate intermediate is completely formed in apparent intermediate B in Figure 6A. The remaining spectral changes in the second phase of the reaction (B→C) are consistent with changes observed in reactions with the other substrates that are attributed to dissociation of the last ligand from the three-coordinate intermediate and slight transfer of electrons from NADPH to FAD; however, the very low rate constant for this phase ($k_{obsB\rightarrow C} = 0.34\ s^{-1}$) may also reflect a requirement for additional conformational changes to allow full dissociation of the remaining bulky cysteine ligand. As in the case of the inhibited complex formed from $Hg(CN)_2$, the λ_{max} of the final NADPH/FAD CT band suggests that, although the *inner* Hg(II) complex is fully formed, a negative charge may remain in the vicinity of the flavin, consistent with the need for protonation of the similarly basic thiolate anion and cyanide ligands upon dissociation.

Reaction of Hg(Cys)$_2$ with CCCC. The presence of the C-terminal cysteines in CCCC enzyme, once again, dramatically alters its reaction in comparison with CCAA enzyme, with the most critical differences being the rapid binding of $Hg(Cys)_2$ and the resultant formation of an intermediate in which Hg(II) is reduced at a catalytically relevant rate. The full time course of the reaction is quite complex and requires a model with five exponentials to fit the data satisfactorily over the entire spectral region (Figure 7B). However, in Figure 7A, we present only the spectral changes associated with binding of $Hg(Cys)_2$ that result in formation of the reducible Hg(II) complex (curve C), and will present a more complete analysis of the ensuing reaction, and factors affecting it, in a forthcoming paper. As illustrated in Figure 7A for the reaction of 0.5 mM $Hg(Cys)_2$ with 29.7 μM CCCC EH_2·NADPH (stoichiometric complex), the typical spectral changes associated with binding of Hg(II) to C140 (partial resolution of the flavin main band and a decrease in thiolate/FAD CT absorbance) are already observed in the deadtime of the measurement (A → B), in distinct contrast to the reaction with CCAA enzyme where essentially no changes were observed in the deadtime (Figure 6A). This binding phase reaches completion at apparent intermediate C, which is the first intermediate obtained from the fit of the data over the full time range (Figure 7B), and is the species from which reduction of Hg(II) ensues. The presence of three isosbestics in the conversion of A → B → C indicates that A → C is a monophasic reaction, and the analysis gives a value of ~220 s^{-1} for $k_{obsA\rightarrow C}$. The spectrum of intermediate C is identical at higher concentrations of $Hg(Cys)_2$ (1.0 and 1.5 mM), but conversion of A → C is nearly complete in the deadtime, once again indicating that the second-order binding reaction is at least partially rate-limiting in this process. Thus, to account for the value for $k_{obsA\rightarrow C}$ of 220 s^{-1} obtained with 0.5 mM $Hg(Cys)_2$, the second-order rate constant $k_{binding}$ must be *at least* $4.4 \times 10^5\ M^{-1}\ s^{-1}$, a value more than 3 orders of magnitude higher than the second-order rate constant for binding to the CCAA enzyme (Table 2). Clearly the C-terminal cysteines provide a pathway for rapid binding of the larger $Hg(Cys)_2$ and transfer to the inner active site that is not available in the CCAA enzyme, a result consistent with the much larger access channel to C558 (C629) than to C135 (C207) apparent in the structure (Figure 1).

Comparison of the spectrum of the reducible intermediate in the CCCC enzyme (Figure 7A, curve C) with that of the

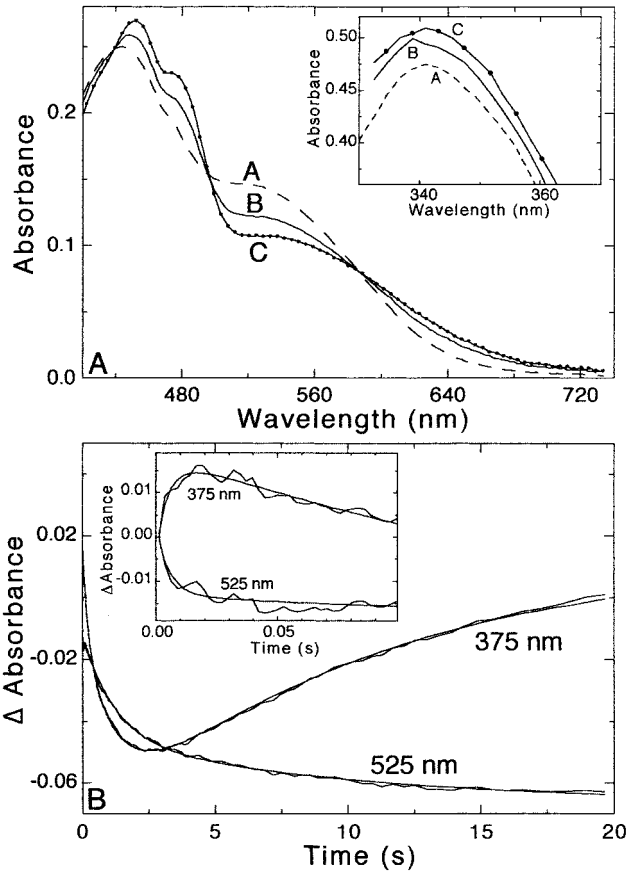

FIGURE 7: Binding of Hg(II) to CCCC EH_2·NADPH using Hg(Cys)$_2$. The EH_2·NADPH complex of wild-type enzyme CCCC (29.7 μM stoichiometric complex, panel A, curve A) was mixed in the stopped-flow spectrophotometer with 0.5 mM Hg(Cys)$_2$ (final concentrations). A model with five consecutive exponentials was required to fit the data satisfactorily. Panel A depicts only the species relevant to the binding event. Curve B reflects the deadtime spectrum (not a discrete intermediate), and curve C is the spectrum after completion of binding. The fit yields an apparent rate constant of 224 s^{-1} for conversion of curve B to C. The *inset* shows changes in the 340 nm region. Panel B shows the time-dependent spectral changes at 525 and 375 nm for the entire reaction described above. The *inset* shows the changes during the first 100 ms of the reaction. The smooth lines were obtained from a fit to five exponentials with apparent rate constants of 224, 80, 5.2, 0.84, and 0.095 s^{-1}, obtained from global analysis of the data.

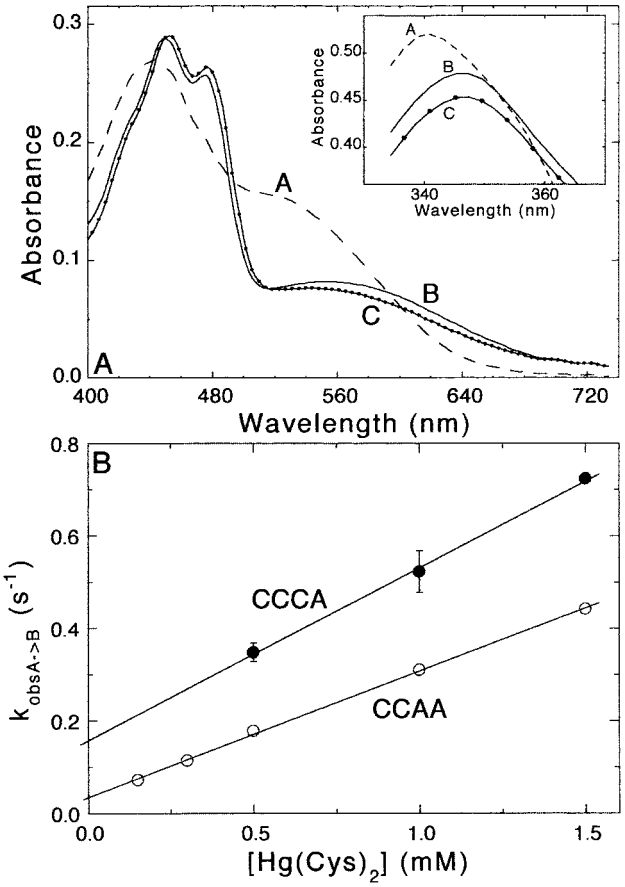

FIGURE 8: Panel A shows results of rapid mixing of 30.5 μM CCCA EH_2·NADPH (curve A) with 1.5 mM Hg(Cys)$_2$ (final concentrations*). No changes occur during the deadtime of the measurement.* Curves B and C are the spectral species obtained from SVD of the raw data and a fit to two consecutive exponentials, with apparent rates of 0.72 and 0.3 s^{-1} for the first and second phases, respectively. The *inset* depicts changes in the 340 nm region. Panel B shows a plot of the apparent rate constants obtained for the first phase versus Hg(Cys)$_2$ concentration. For comparison the analogous plot obtained for the CCAA enzyme, taken from Figure 5, is also shown.

inhibited complex in the CCAA enzyme derived from either Hg(Cys)$_2$ (Figure 6A, curve C) or Hg(CN)$_2$ (Figure 2A, curve D) shows that the binding-induced quenching of the thiolate/FAD CT absorbance in the reducible intermediate is only about half that observed in the inhibited complex. Thus, it appears that, when binding of an HgX_2 substrate is limited to the C-terminal access route by the size of the ligand X, rapid transfer of Hg(II) to the *inner* complex involving the C140 sulfur only occurs in 50% of the sites. Recall that this is similar to the 50% quenching observed in the initial reaction of CCAA enzyme with Hg(CN)$_2$ (Figure 2A), suggesting that it may be due to a simple equilibration of bound Hg(II) among the *inner*, *middle*, and *outer* two-coordinate complexes (Scheme 2). However, the ensuing consumption of NADPH, concomitant with reduction of Hg(II), occurs biphasically, a result that cannot be explained by a simple equilibrium model, but may be consistent with an asymmetric dimer model as previously proposed (*24*). Further evaluation of this reaction and the factors affecting it and a thorough consideration of both linear and asymmetric kinetic models will be presented in a forthcoming paper. At this point, the major conclusion to be drawn from the data is that formation of a reducible *inner* complex, starting from an HgX_2 substrate with high-affinity, basic X ligands, requires access via the C-terminal route to remove those ligands before entering the inner active site. On the basis of the energy of the remaining NADPH/FAD CT absorption band in the inhibited complexes, it is proposed that this may be necessary to prevent development of negative charge in the vicinity of the *inner* complex as the last basic ligand dissociates, since such a charge would be expected to disfavor electron transfer into the metal ion binding site from the flavin. This hypothesis further suggests that other residues in the C-terminal access channel may play a critical role in transferring protons between the attacking enzyme thiols and the dissociating X ligands, an idea we are currently investigating.

Binding of Hg(Cys)$_2$ to CCCA. As one final step to verify the analysis of binding pathways in the structure, we also have examined the reaction of Hg(Cys)$_2$ with the CCCA enzyme, which lacks the most surface-exposed cysteine in

the C-terminal pathway, C558 (C629, Figure 1). Comparison of the spectral changes for this reaction shown in Figure 8A with those for the CCAA enzyme in Figure 6A indicates a similar outcome in the two proteins. Thus, binding to the C140 sulfur goes to completion, yielding an inhibited complex in a $[Hg(Cys)_2]$-dependent reaction with a second-order rate constant $k_{binding}$ of 370 M^{-1} s^{-1} (Figure 8B). These results clearly indicate an absolute requirement for C558 to achieve the rapid binding and transfer of Hg(II) to the inner active site from bulky HgX_2 substrates, which is consistent with the requirement for all four cysteines for in vivo activity where MR is expected to encounter bulky $Hg(SR)_2$ complexes.

SUMMARY

From the results presented here, together with the results in the previous study with $HgBr_2$, we can draw several conclusions. First, the route of entry for an HgX_2 substrate depends on the size of the ligand X. Large ligands allow *rapid* access to the active site only via the C-terminal route, while small ligands allow rapid access by both the C-terminal and bypass routes highlighted in Figure 1. Second, an *inner* two-coordinate complex can be formed via either route. When entry is via the bypass route, the *inner* complex appears to be formed completely in both active sites; however, the spectrum and reducibility of the final *inner* complex depend on the affinity/basicity of the last X ligand to be displaced. Low-affinity/basicity ligands such as bromide dissociate to give rapidly reducible complexes, while high-affinity/basicity ligands dissociate to give inhibited complexes. The difference in spectral properties of the two complexes suggests the presence of a negative charge in the vicinity of the final inhibited *inner* complex, consistent with the need for protonation of the more basic dissociating ligand. Finally, entry via the C-terminal route appears to prevent development of this negative charge for high-affinity/basicity ligands since the *inner* complex formed via this route is reducible at a catalytically relevant rate. However, formation of the *inner* complex does not go to completion when this is the only route of entry (i.e., when X is large); instead, an apparently asymmetric complex is formed. Because this is unquestionably the relevant route of entry for the expected bulky $Hg(SR)_2$ substrate under physiological conditions, we are pursuing further studies to explore the factors leading to this apparent asymmetry, and to determine the importance of it to the catalytic cycle with bulky HgX_2 substrates.

ACKNOWLEDGMENT

We thank Emil Pai for sharing the coordinates of MR from *Bacillus sp*. RC607 and Jennifer L. Harris (C. Craik lab) for access to their computer graphics system.

REFERENCES

1. Stricks, W., and Kolthoff, I. M. (1953) *J. Am. Chem. Soc. 75*, 5673−5681.
2. Miller, S. M. in *Essays in Biochemistry* (Ballou, D. P., Ed.) Vol. 34, Portland Press Ltd., London, U.K. (in press).
3. Miller, S. M., Moore, M. J., Massey, V., Williams, C. H., Jr., Distefano, M. D., Ballou, D. P., and Walsh, C. T. (1989) *Biochemistry 28*, 1194−1205.
4. Schiering, N., Kabsch, W., Moore, M. J., Distefano, M. D., Walsh, C. T., and Pai, E. F. (1991) *Nature 352*, 168−172.
5. Distefano, M. D., Moore, M. J., and Walsh, C. T. (1990) *Biochemistry 29*, 2703−2713.
6. Sahlman, L., Lambeir, A.-M., Lindskog, S., and Dunford, H. B. (1984) *J. Biol. Chem. 259*, 12403−12408.
7. Miller, S. M., Ballou, D. P., Massey, V., Williams, C. H., Jr., and Walsh, C. T. (1986) *J. Biol. Chem. 261*, 8081−8084.
8. Sandström, A., and Lindskog, S. (1988) *Eur. J. Biochem. 173*, 411−415.
9. Rennex, D., Pickett, M., and Bradley, M. (1994) *FEBS Lett. 355*, 220−222.
10. Distefano, M. D., Au, K. G., and Walsh, C. T. (1989) *Biochemistry 28*, 1168−1183.
11. Moore, M. J., and Walsh, C. T. (1989) *Biochemistry 28*, 1183−1194.
12. Moore, M. J., Miller, S. M., and Walsh, C. T. (1992) *Biochemistry 31*, 1677−1685.
13. Raybuck, S. A., Distefano, M. D., Teo, B.-K., Orme-Johnson, W., and Walsh, C. T. (1990) *J. Am. Chem. Soc. 112*, 1983−1989.
14. Marshall, J. L., Booth, J. E., and Williams, J. W. (1984) *J. Biol. Chem. 259*, 3033−3036.
15. Miller, S. M., Massey, V., Ballou, D. P., Williams, C. H., Jr., and Walsh, C. T. (1987) *Flavins and Flavoproteins*, pp 29−32, Walter de Gruyter & Co., Berlin, New York.
16. Engst, S., and Miller, S. M. (1998) *Biochemistry 37*, 11496−11507.
17. Skoog, D. A., West, D. M., and Holler, F. J. (1988) *Fundamentals of Analytical Chemistry*, 5th ed., pp 819−820, Saunders College Publishing, Fort Worth, TX.
18. Cheesman, B. V., Arnold, A. P., and Rabenstein, D. L. (1988) *J. Am. Chem. Soc. 110*, 6359−6364.
19. Bowmaker, G. A., Dance, I. G., Dobson, B. C., and Rogers, D. A. (1984) *Aust. J. Chem. 37*, 1607−1618.
20. Lawton, S. L. (1971) *Inorg. Chem. 10*, 328−335.
21. Levason, W., and McAuliffe, C. A. (1979) in *The Chemistry of Mercury* (McAuliffe, C. A., Ed.) pp 49−115, The MacMillan Company of Canada Ltd., Toronto.
22. Dean, J. A. (1992) *Lange's Handbook of Chemistry*, 14th ed., McGraw-Hill, Inc., New York.
23. Fox, B., and Walsh, C. T. (1982) *J. Biol. Chem. 257*, 2498−2503.
24. Miller, S. M., Massey, V., Williams, C. H., Jr., Ballou, D. P., and Walsh, C. T. (1991) *Biochemistry 30*, 2600−2612.
25. Schultz, P. G., Au, K. G., and Walsh, C. T. (1985) *Biochemistry 24*, 6840−6848.

BI982680C